Expanded View Figures

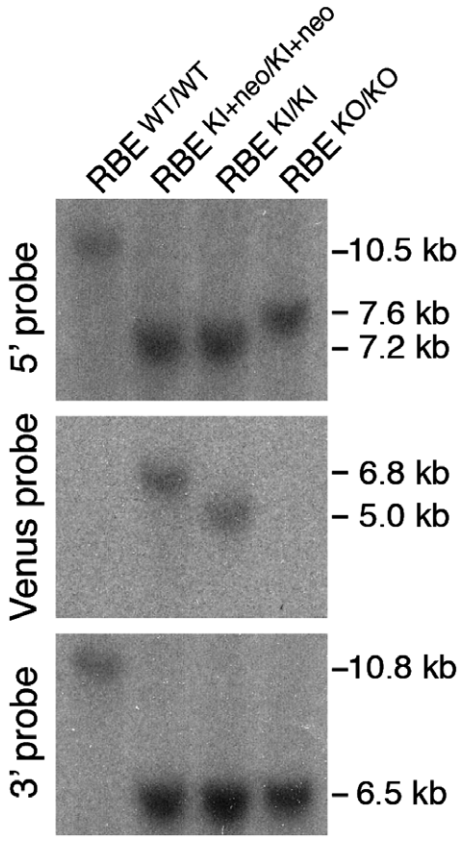

Figure EV1. Southern blotting analysis of homologous recombination.
Southern blot analysis of genomic DNA from homozygous wild-type (RBE^{wt}) and mutated alleles of RIBEYE (RBE^{KI+neo}, RBE^{KI}, and RBE^{KO}; see Fig 1A). Correct recombination events were confirmed using outside probes hybridizing to the 5′ (*Sac*I-digested genomic DNA) and the 3′ homology region (*Bam*HI digested) and to the GFP-coding portion of GCamP3 (Venus probe; *Bam*HI digested). Positions of size markers are indicated on the right.

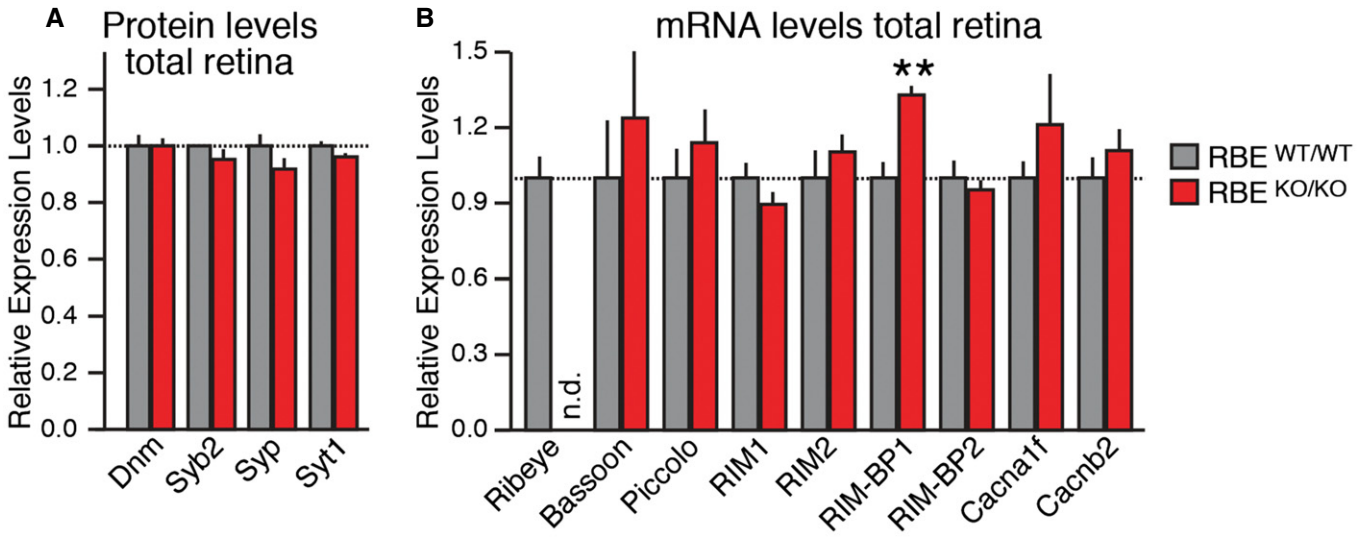

Figure EV2. Protein and mRNA expression analysis of RIBEYE mutant mice.

A Levels of additional synaptic proteins in retina homogenates from littermate $RBE^{WT/WT}$ and $RBE^{KO/KO}$ mice complementing those shown in Fig 1F. Levels were determined by quantitative immunoblotting using fluorescently labeled secondary antibodies; results are normalized to loading controls depending on molecular weights (actin, VCP, and GDI) and to wild-type controls.

B Quantitative RT–PCR analysis of a series of presynaptic proteins in total retina from littermate $RBE^{WT/WT}$ and $RBE^{KO/KO}$ mice. Levels were standardized on actin transcript levels and relative to wild type.

Data information: Data are presented as mean ± SEM; statistical analyses were performed using Student's *t*-test (**$P < 0.01$; $n = 4$ mice per genotype).

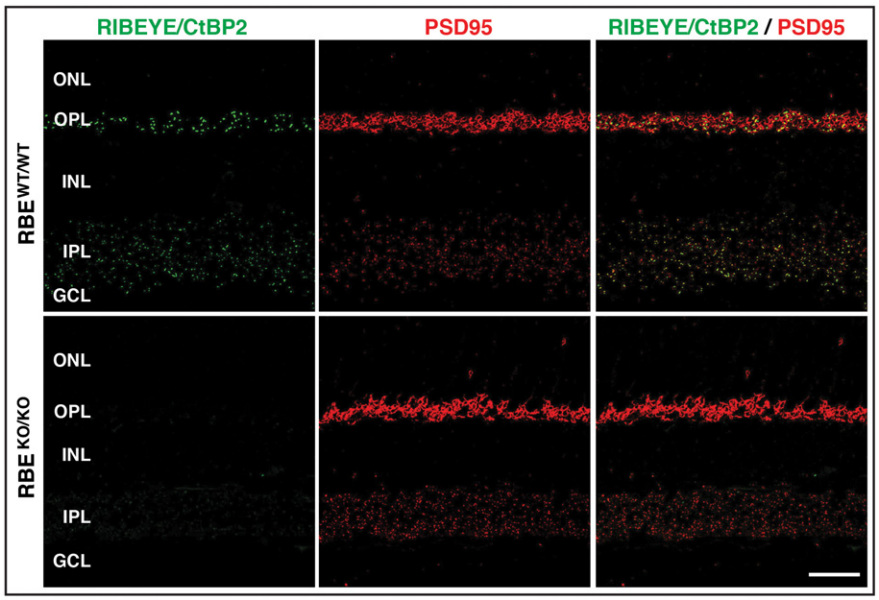

Figure EV3. Immunofluorescence staining of RIBEYE/CtBP2 and PSD95 in wild-type and RIBEYE KO retina.

Representative double immunofluorescence labeling of RIBEYE/CtBP2 (green, to label the B-domain common to both splice forms) and PSD95 (red) in semi-thin sections of $RBE^{WT/WT}$ and $RBE^{KO/KO}$ retina. The $RBE^{KO/KO}$ retina clearly shows a lack of RIBEYE in photoreceptor terminals in the outer plexiform layer and bipolar cell terminals in the inner plexiform layer compared to wild-type retina. Scale bar: 20 μm; abbreviations: ONL, outer nuclear layer; OPL, outer plexiform layer; INL, inner nuclear layer; IPL, inner plexiform layer; GCL, ganglion cell layer.

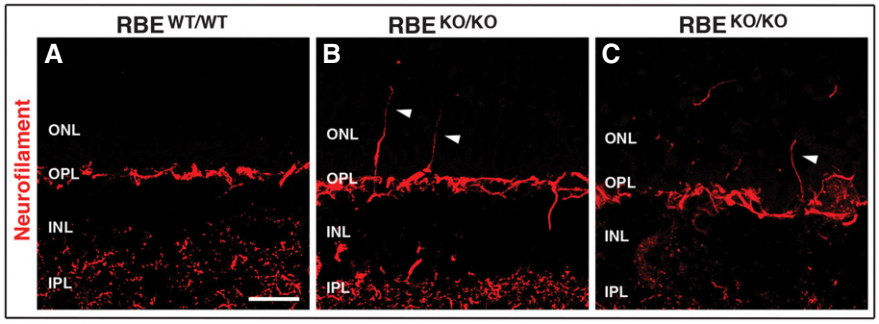

Figure EV4. Aberrant sprouting of horizontal cell processes in the ONL of *RBE$^{KO/KO}$* mice.

A Representative immunofluorescence staining of neurofilament (red) in the OPL and IPL of retinas in *RBE$^{WT/WT}$*. Scale bar: 2 μm.

B, C Examples of aberrant processes of horizontal cells sprouting into the ONL of *RBE$^{KO/KO}$* mice (white arrowheads). Images are 4-μm z-stack projections.

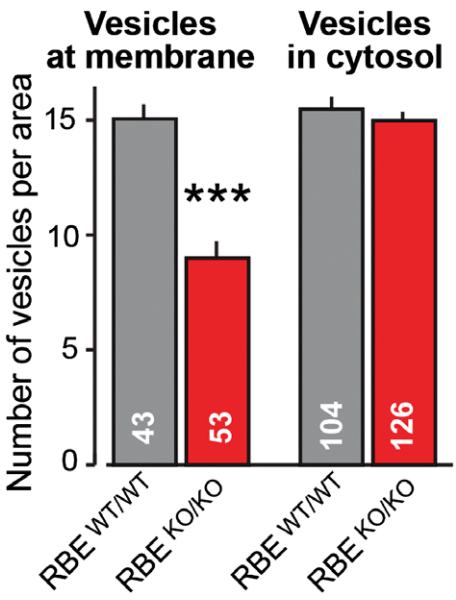

Figure EV5. RIBEYE KO causes a loss of synaptic vesicles.

Average vesicle density (expressed as vesicle numbers per rectangle or square, respectively, see Fig 5A and B) in the area adjacent to synaptic junctions or the cytosol. Statistical analyses were performed using Student's *t*-test; data are presented as mean ± SEM (***$P < 0.001$; numbers of analyzed synapses are indicated in the bars).

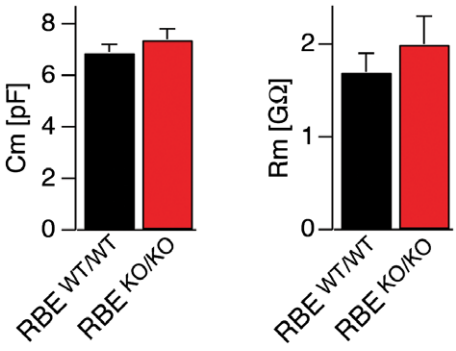

Figure EV6. Capacitance and input resistance values of patched retinal AII amacrine cells.

Neuronal capacitance (left) and input resistance (right) recorded from AII amacrine cells of *RBE$^{WT/WT}$* and *RBE$^{KO/KO}$* mice. Data are presented as mean ± SEM; numbers of cells analyzed are the same as for Fig 6. No statistical significance was observed between wild-type and KO cells as assessed by Student's *t*-test.